Appendix B (text fragments)

Appendix B1: Detailed sample description

Samples from the Schwarzwald (Black Forest, BF)

Samples were taken from the Rappenloch mine, the Schrotloch mine, and the Schloßberg Gegentrum mine in the Schwarzwald Mining District, SW Germany. At Rappenloch, previous investigations already noted the elevated W concentrations in hematite and goethite (Faisi 1951; Wimmenauer 1955; Metz 1977; Pfaff et al. 2009). These botryoidal iron ores were presumably formed during the oxidation of primary iron(II)-bearing minerals within hydrothermal veins (Markl et al. 2006). Based on field observations and fluid inclusion investigations, temperature of formation is close to surface conditions for the Freiamt and between 50 and 150 °C for the Eisenbach locality (Lüders 1994; Baatartsogt et al. 2007). For the Schrotloch locality, the temperature of formation remains unclear. The overall botryoidal habits, however, imply that these samples formed as cavity fillings and share a similar mode of origin (cf. Fig. B1). The following discusses the prevailing differences of the sample localities, namely their formation age, tectonic setting, primary mineral assemblage, and linkage to minor W-mineralization:

Hematite BF-11. This sample comes from the Rappenloch mine, which is part of the Eisenbach mining area located in the eastern part of the central Schwarzwald. All veins strike SE to ESE on both sides of a local fault zone within a granitic host rock right below the basement-cover unconformity. Wernicke and Lippolt (1993) determined a Middle to Late Jurassic hematite formation age at this locality. The reconstruction of the former overburden (~550 m) and epithermal temperatures suggest a hypogene origin of the ores. The paragenetic sequence is complex with repetitive stages, involving the successive crystallization of quartz, barite, hematite and different manganese-oxi/-hydroxides (Faisi 1951; Wimmenauer 1955; Schatz 1970). W is known to occur in significant concentrations in hollandite and as intergrowth of scheelite with hematite and other manganese ores (Kirchheimer 1953; von Gehlen 1958; Walenta 1963; Schatz 1970; Werner et al. 1990). Sample BF-11 consists of a botryoidal hematite which splits into three distinctive texture types (Fig. B1a-b).

Hematite and goethite BF-26. This specimen originates from the Schrotloch mine near Unterstmatt in the northern Schwarzwald. The local mine extracted ore from the ESE-striking hydrothermal vein within the granitic host rock and contains a quartz gangue (Metz 1977) with botryoidal and massive fibrous hematite/goethite. The vein crosscuts the overburden Early Triassic cover rocks. Hematite has been dated to be Late Triassic (Wernicke and Lippolt 1995). Fresh iron-bearing minerals of an earlier mineralization stage have not been found so far, but rare botryoidal supergene goethite shows perimorphs after siderite. It is unclear, whether the botryoidal hematite is also of supergene or rather of hypogene origin. Textural and geological

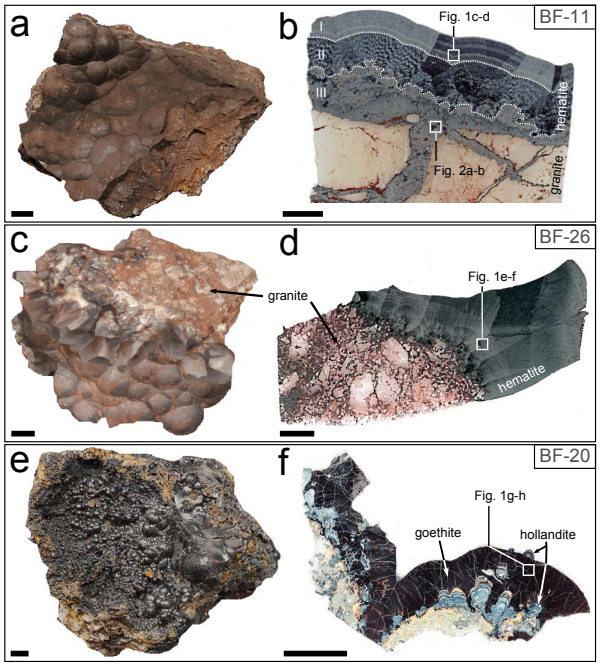

Figure B1: Photographs of the botryoidal iron ore samples from the Schwarzwald Ore district (left side) and the corresponding thin sections used in this study (right side). (**a-b**) Sample BF-11; Rappenloch mine of three textural generations: (I) a highly porous hematite mixture occupies and crosscuts the former intensively silicified granite is followed by a (II) feather-like and (III) a more layered hematite. On microscopic scale the porous hematite can be subdivided into early, porous, and globular aggregates (Fig. 1a; hem-I), overgrown by a feathered hematite (Fig. 1a; hem-II) texturally equal to that in Fig. B1b. The morphology of relic siderite is still recognizable. (**c-d**) Sample BF-26; Schrotloch mine: more fibrous, botryoidal hematite sitting upon granite intensively infiltrated by hematite. (**e-f**) Sample BF-20; Schloßberg-Gegentrum mine: mostly uniform botryoidal goethite in intergrowth to hollandite. Scale bar is 5 mm.

similarities to the Rappenloch occurrence and an overburden thickness of about 575 m at the time of hematite formation (Late Triassic), however, suggests a hypogene origin. In the Schrotloch mine and in the whole northern Schwarzwald, tungsten mineralizations are unknown (Werner et al. 1990). In contrast to the Rappenloch deposit, the hematite sample shows a more uniform and fibrous-shaped hematite with minor layers caused by changing porosity (Fig. B1c-d). The main mass of goethite in the vein occurs separated from hematite on a second, cross cutting fault. However, this goethite is intergrown with small amounts of paragenetic hematite.

Goethite BF-20. The specimen comes from the Schloßberg-Gegentrum mine in the western part of the central Schwarzwald (Freiamt mining area). This former mining site is located right at the mineralized Rhinegraben boundary fault which has a Paleogene age and strikes about NNE (Werner and Franzke

1994). Along the fault, basement gneisses were tectonically juxtaposed to the Triassic sandstone cover rocks. According to Metz et al. (1957), the primary generation of quartz, siderite, barite, galena, chalcopyrite, sphalerite and tennantite is followed by supergene quartz, botryoidal goethite, minor pyrolusite, and further manganese oxides (here identified as hollandite). The closest evidence for a W-mineralization is in the Heuberg rhyolite about 5 km NNW (Werner et al. 1990), where scheelite crystals have been found in open vugs. The sample BF-20, shown in Fig. B1e-f, consists of a mostly uniform botryoidal sequence of goethite which is intergrown with two generations of hollandite. Both phases overgrow a fine-grained mixture of quartz, barite, goethite, and hollandite.

Samples from the Grantcharitza deposit (GR)

Tarassov et al. (2002) have already examined the samples from the W-deposite Grantcharitza with a series of methods including EMPA, Raman spectroscopy, and XRD. This deposit is situated in the Western Rhodope Mountains, 18 km SW from the town of Velingrad (Plovdiv region, Bulgaria). The deposit penetrates porphyritic granites and granodiorites of the composite Rila-Western Rhodope Batholith (central part of West Rhodope Mountains) (Kamenov et al. 1999). The ore zone lies subparallel to the most important tectonic structure in the region. The ore mineralization occurs in pegmatoid quartz-feldspar veins and in the wallrock as disseminated ores. Scheelite and pyrite occur as the stable primary paragenetic ore association. Earlier works also reported rare findings of wolframite ($[Fe,Mn]WO_4$) and ferberite ($FeWO_4$) (Dimitrov 1981). The Grantcharitza ore is considered as high-temperature hydrothermal scheelite deposit, which got partly weathered (Dimitrov 1981). Samples used in this study were comprised of glassy compact goethite masses (plus minus hematite). These goethite masses occupy the fractures and cavities in quartz and feldspar, remaining after pyrite and scheelite dissolution. Tarassov et al. (2002) distinguished two generations of goethite (G-I and G-II) and one generation of a W-rich phase (F_W) by their different W concentration. In addition, hematite (H-I) exists. Due to its micro scale intergrowth, XAFS measurements were only possible on the G-I goethite generation. Sample denomination $GR_{G\text{-}I}$, $GR_{G\text{-}II}$ and $GR_{H\text{-}I}$ are used for the phases mentioned above, respectively. Own microscopic observations revealed that both phases, $GR_{G\text{-}I}$ and $GR_{H\text{-}I}$ are fragments of laminated and botryoidal aggregates, which were cemented by $GR_{G\text{-}II}$ later. Although $GR_{G\text{-}I}$ and $GR_{H\text{-}I}$ show comparable textural features their temporal relation to each other are still uncertain.

APPENDIX B2: SYNTHESIS OF FERRIHYDRITE SUSPENDED KOH SOLUTION

For ferrihydrite synthesis a mass of 5.05 g Fe(NO3)3•9H2O was dissolved in 100 mL deionized water and transformed into ferrihydrite by adding 22.5 mL 5 M potassium hydroxide (KOH) solution rapidly under constant agitation. In order to reduce the remaining K and NO_3, associated with ferrihydrite, the precipitate was washed gradually with about 8 L of deionized water until the conductivity of the suspension arrived below 60 µS/m. Consecutively, the volume of the ferrihydrite suspension was reduced to 100 mL by decantation and the pH was adjusted to 4 by adding HNO3 (50 %) for hematite synthesis, or pH 12 by adding KOH (5 M) for goethite synthesis. These ferrihydrite suspended KOH solutions were spiked with different molar W concentrations (see chapter 2.3).

APPENDIX B3: XANES AND EXAFS METHODS

The decreasing of the intermediate focus width at the Si(111) monochromator crystal configuration was preferred for XANES measurements, because improvement of energy resolution was similar and moving slits is less time consuming than moving to the Si(311) crystals because subsequent W L_3 EXAFS measurements were also performed with the Si(111) crystal pair (see chapter 3.7).

XANES and EXAFS spectra were energy calibrated with an Au-foil (11.919 eV: 1st derivative of the Au L3 edge spectrum) and Fe-foil (7.112 keV: 1st derivative Fe K-edge spectrum) between the ionization chambers 2 and 3, respectively, pre- and post-edge background corrected with a linear and a polynomial function of third degree, respectively, and normalized to an edge jump of one to compare spectra of different samples using the ATHENA program of the IFFEFIT package (Ravel and Newville 2005).

For transmission mode ionization chambers and for fluorescence mode a seven element Si(Li) solid state detector (SGX Sensortech) were used to record the W $L\alpha_1$ (W L_3 edge), $L\gamma_1$ (W L_1 edge) and Fe Kα (Fe K edge) fluorescence emission intensity.

W L_1 µ- XANES spectra have only been measured from the natural, W-rich hematite BF-26 on thin section and on pellets from separated material. For the goethite BF-20 which contains less W than the hematite the fluorescence emission intensity was not sufficient for recording spectra with a good signal to noise ratio within reasonable time

For all XANES and EXAFS measurements up to 20 scans have been recorded to get reliable signal to noise level depending on the W content of the samples. Step width for the XANES and EXAFS spectra were 5 eV (-150 to -50 eV related to the edge) and 2 eV (-50 to -20 eV) for the pre-edge background, 0.3 eV across pre-edge and XANES region (-20 to 20 eV), k steps of 0.05 eV-1 up to k=14 with acquisition time 0.44*k s in the EXAFS region for W L3-edge, k=12 with k0.5 s for W L1-edge, and up to k=12.4 for Fe K-edge with acquisition time 1 s. For measurements with the Si(311) monochromator crystal pair 0.2 eV step width has been chosen across the edge.

Fe K XANES spectra from the thin section had to be measured in fluorescence mode because the thin section is intransparent tor the X-ray beam. Due to the high Fe concentration spectra are strongly damped and have been self absorption corrected using the algorithm implemented in the ATHENA program (Ravel and Newville 2005). Spectra of wolframite and reference goethite and hematite were measured in transmission at pellets as well as spectra of synthetic W-containing goethite and hematite.

To extract the energy gap of the W L_3-edge spectra they were fitted with a tangens function to simulate the edge and two Voigt peak functions for the composite whiteline similar as described in Yamazoe et al. (2008). W L_1-spectra were fitted with tangens function as described and one or two Lorentz peaks to extract the pre-edge area also according to Yamazoe et al. (2008). The fits have been performed with the program fityk (Wojdyr, 2010). Results of the fits are shown in Fig. A4.1, A4.2. Additionally, the

second derivatives of the W L_3 XANES have been calculated for comparison with the W L_3 whiteline peak fits (Fig. A3).

APPENDIX B4: XANES RESULTS

Analysis of the W L_3 whiteline split by peak deconvolution results in about 2.5 eV for $Na_2WO_4 \cdot 2\ H_2O$, 2.7 eV for $CaWO_4$, 3.7 eV for hübnerite, and 3.9 for wolframite. Split values for natural goethite BF-20 and synthetic goethite SYN-$goe_{0.05;25°C}$ are about 3.5 eV, and for the natural and synthetic hematites (BF-26, SYN-$hem_{0.5}$) are about 4 eV. Similar results have been found also from the analysis of the second derivatives of the W L_3 XANES spectra.

APPENDIX B5: EXAFS RESULTS

For fitting of the EXAFS spectra of W-goethite and W-hematite, we used the crystal structures of Gualtieri&Venturelli (1999) (goethite) and Blake et al. (1966) (hematite), in which one W replaces one Fe. Before replacing Fe by W, the structure was transformed to space group *P1* to remove all symmetry operators. After calculating the individual paths using the software FEFF6 (de Leon et al. 1991), implemented in the Artemis software package, the amplitude of all paths was restrained to one and not refined during the whole fitting procedure. Therefore, all paths share one common value for amplitude.

For goethite and hematite, the first six oxygen atoms were fit with two W-O paths, of four and two oxygen atoms. This procedure was necessary due to the strong distortion of the WO_6-octahedron (see results). Both paths share the same amplitude and Debye-Waller factor (σ^2), but possess individual values for Δr (see Table 3.1 for goethite and 3.2 for hematite). The successive Fe and O atoms where fit with two additional Δr in case of goethite and up to three Δr for hematite.

In order to reduce the number of variables during the fit, paths beyond the first two W-O paths were partially fit with Δr values of the first and second W-O path. Additionally, the background correction, implemented into the Artemis software package, was used, adding seven additional variables. The number of variables can therefore be calculated by the following equation:

$$N_{var} = \Delta E_0 + \text{amplitude} + \Sigma\Delta r + \Sigma\sigma^2 + 7$$

APPENDIX B6: XANES DISCUSSION

The major contribution to the W L_3 edge spectra arises from the $2p_{3/2}$ to 5d transition. A whiteline splitting as it is observed for Mo and W compounds corresponds to the ligand field splitting of the d-orbitals. The pre-edge intensity in the W L_1 XANES spectra arises from forbidden electron transitions that become allowed due to the mixing of the p orbitals of tungsten and the ligand into empty d orbitals. Both these parameters contain information on the W structure. They show a linear relationship that can be used to distinguish between W in tetrahedral as well as undistorted and distorted octahedral coordination (Yamazoe et al., 2008).

Surprisingly, the W L_3 whiteline split of the synthetic goethite SYN-$goe_{0.05;70°C}$ is similar to the synthetic hematite SYN-$hem_{0.05}$ and the natural hematite BF-26 (all about 4 eV) whereas the split for the synthetic goethite SYN-$goe_{0.05;25°C}$ and the natural goethite BF-20 is ~ 3.5 eV (see Fig. A4.1). The difference of ~0.5 eV at the W L_3 whiteline split shows that the higher synthesis temperature may decrease the final distortion of the WO_6 octahedra in the goethite structure. A compositional dependence is unlikely because tungsten contents are similar in both synthetic goethites from a molar W/Fe ratio of 0.05 (cf. Table 1). A higher synthesis temperature, however, seems to decrease the disorder around the newly incorporated W and results in a less disordered WO_6-octahedron. All prominent features occurring in the W L_1 XANES region besides the pre-edge in Fig. 4 are discussed in Appendix B6.

In the diagram of W L_1 pre-edge area intensity vs. W L_3 whiteline split (Fig. A8) the positions of hübnerite, wolframite and of the two samples natural hematite BF-26 and synthetic goethite SYN-$goe_{0.05;70°C}$ are located about half the way from the lower right corner that represents a regularly octahedral coordination like in Ba_2NiWO_6 or Cr_2WO_6 (Yamazoe et al., 2008) to the upper left corner which stands for tetrahedral coordination as in $Sc_2W_3O_{12}$ or $NaWO_4$ (Yamazoe et al, 2008), $NaWO_4 \cdot 2H_2O$ (this study). Compounds that plot between the "end members" like WO_3, $H_3PW_{12}O_{40} \cdot 13H_2O$, $(NH_4)_{10}W_{12}O_{41} \cdot 5H_2O$ (Yamazoe et al., 2008) or hübnerite and wolframite (this study) and our samples are then characterized by a distorted octahedral structure.

Due to the low W content of natural goethite BF-20 no W L_1 edge spectrum has been recorded. It is expected that it plots slightly towards the upper left corner because its W L_3 whiteline split of 3.5 eV is about 0.5 eV smaller than for the natural hematite (4 eV) indicating a somewhat higher octahedral distortion. An energy gap between 3.5 and 4 eV results in a mixing ratio of empty 6p into 5d orbitals of about 10 % using the calibration of Yamazoe et al. (2008, their Figure 12). Their calibration comprises structures from undistorted (Cr_2WO_6) to largely distorted octahedra as in $H_3PW_{12}O_{40}$ x 13 H_2O. The latter correspond to 20 % orbital mixing. Hence, 10 % mixing means a significant distortion of the octahedra in the structures of our samples. A more precise determination of the mixing ratio is difficult due to some scatter of the data points in the calibration diagram of Yamazoe et al. (2008).

Besides the pre-edge (Fig. 4: A) the W L_1 XANES region of the sample spectra is characterized by more prominent features (Fig. 4: B, C and D). The first feature (B) can be assigned to the edge: 2s(W) to 6p(W) transition into the continuum (Kuzmin and Purans 1993). The second feature could be discussed in terms of multiple scattering. For example, Kuzmin and Purans (1993) distinguished two more features (Fig. 4: C and D) besides the edge (Fig. 4: B) in the W L_1 spectra of their WO_{3-x} (x = 0 to 1) series and assigned single scattering and first shell multiple scattering to features B and D, and single and multiple scattering from the W atoms in the second shell to feature C. Additionally, they have shown that the L_2 edge EXAFS contribute to the L_1 edge because both edges are just separated by 556 eV. The presence of Fe instead of W as a second neighbor, as it is assumed for our samples, may shift the intensity distribution across the XANES region in a way that inhibit a C feature as mentioned above. However, for a deeper understanding of the XANES features that are related to multiple scattering, a theoretical approach is required.

APPENDIX B7: ADDITIONAL METHODS

Electron microprobe analysis (EMPA)

Elemental composition of the natural and synthetic samples was determined using a JEOL JXA-8900RL electron microprobe in wavelength-dispersive mode at the Fachbereich Geowissenschaften of the University of Tübingen, Germany; quantitative element distribution maps of W were additionally obtained on a JEOL JXA-8230 at the Institute of Geosciences, Friedrich-Schiller-University Jena, Germany. Natural and synthetic standards were used for calibration, the exact specifications can be found in Table A1 of Appendix A. For focused beam measurements, a beam current of 20 nA and an acceleration voltage of 20 kV were used. For element maps, a beam current of 50 nA, an acceleration voltage of 20 kV, and a dwell time of 300 ms/pixel were used to reach comparable count rates.

Although most samples showed no problems during the WDX analyses, the synthetic iron oxides showed low totals due to their high porosity. The chemical composition of all synthetic samples was therefore additionally investigated by total reflection X-ray fluorescence spectrometry (TXRF) (see below).

Supplemental Table 1 shows the EMPA data of the synthetic and natural powder samples, which were also used for refinement of crystallographic parameters; Table 2 shows the EMPA data of the natural hematite and goethite samples BF and GR, respectively.

Powder X-ray diffraction (pXRD)

For phase identification and crystallographic parameters, powder X-ray diffraction (pXRD) patterns of all synthetic samples, the natural sample BF-26, and the reference compounds were collected with a Bruker D8 AXS Advance diffractometer with Cu Kα radiation (λ = 1.54058 Å) at the Friedrich-Schiller-University Jena, Germany. The patterns were collected at 20 °C between 5-130 °2θ with a step size of 0.02 °2θ and a dwell time of 1 second. For refinement, the patterns of all samples were processed with the program TOPAS®, where a fitting range between 15-130 °2θ was chosen. For each fit, the statistical measures from the obtained data are given including the residuals for the weighted profile (R_{wp}) and the goodness-of-fit (GOF) (see Supplemental Table 1). For sample BF-26, predefined regions of the botryoidal hematite, previously investigated by EMPA, were ground in an agate mortar (cf. Supplemental Table 1; sample aliquots BF-26 I-VII). However, due to the small sample size and volume, all other goethite samples had to be analyzed by micro X-ray diffraction (see next chapter).

Micro-resolved X-ray diffraction (μXRD)

Due to dilution effects during the preparation of the natural powder samples, resulting in low W contents, additional micro X-ray diffraction analyses were performed in regions of the thin sections with the highest W concentrations to exclude a potential intergrowth of discrete W-bearing impurities. For the regions of interest, the spots with maximum W concentration, previously determined by EMPA, were chosen. All μXRD measurements were performed on thin sections of sample BF-11, BF-20, and BF-26 with a Bruker D8 Discover GADDS theta-theta microdiffractometer at the Fachbereich Geowissenschaften, Universität Tübingen, Germany. To prevent iron fluorescence, a Co-anode with Kα radiation (λ = 1.79 Å) was used at 30 kV and 30 mA with a HOPG monochromator and monocapilarry optics of 500 μm with a 200 μm pinhole. The incident angle to the samples was fixed to 10°. For the general area detector diffraction system (GADDS) a Bruker VÅNTEC500 detector was used and the patterns were integrated between 5-68 °2Θ. Selected μXRD-patterns can be found in Fig. A1 of Appendix A.